ChemComm

COMMUNICATION

View Article Online
View Journal | View Issue

Cite this: *Chem. Commun.*, 2014, 50, 13936

Received 20th July 2014,
Accepted 9th September 2014

DOI: 10.1039/c4cc05597g

www.rsc.org/chemcomm

A cost-effective pH-sensitive release system for water source pH detection†

Zhaoliang Zheng,*[a] Xing Huang[b] and Dmitry Shchukin*[a]

A facile and cost-effective strategy has been developed to form basic cobalt carbonate nanovalves at the orifice of mesoporous nanocontainers, which facilitate the pH sensitive release of functional cargo for up-scaling towards applications in water source pH detection.

Introducing micro- or nano-level design into smart devices for feedback-controlled release has gained a significantly remarkable advancement in the fields of pharmacology and molecular biology than in other fields. The increasing concern about the well-being of humans attracted research in drug delivery or targeted therapy from fundamental studies to the clinic.[1] In contrast, a few successful examples to deliver fertilizers, herbicides and pesticides in agriculture,[2] corrosion inhibitors and antifouling agents in protective coating,[3] and sensory materials[4] in environmental detection have only proven to be useful in the lab. Particularly, environmental biologists found that fish eggs would not hatch in water with a pH lower than 5. Biodiversity also is gradually reduced as lakes and rivers become more acidic.[5] The widespread application of low-cost, stable and easy-to-handle pH sensitive detectors is urgently needed. However, a large gap between the conditions at the research level and the demands for large-scale applications appears because of the limitations of the existing manufactured technologies and cost of raw materials.

Functionalized mesoporous materials have been adopted as an ideal platform for exploring novel approaches for forming feedback release systems that can "survive" under considerably harsher conditions than the *in vivo* environment. They provide a relatively stable porous structure and numerous available functionalizing agents, cargo molecules and strategies to seal the orifice. They are also potentially applicable in scaling-up the production because it is convenient to find natural alternatives for synthetic materials, *e.g.* halloysite nanotubes.[6] To date, we could not find any convincing work on the optimization of various important factors towards scaling-up the production. Tarn *et al.*[7] designed a nanogate that can be simply blocked by forming a strong chelate complex between two orifice-immobilized iminodiacetic acids and a cobalt ion. Massive leakage of cargo would be inevitable if the process of closing the nanogate takes too long, which causes an adverse impact because of the premature exposure of the functional molecules. To minimize any premature release, Lvov's group reported the use of a stopper at the opening end of the halloysites using quick complexation between the loaded benzotriazole (BTA) and the copper ions.[8] Closing the orifice took place in only one minute, but was exclusively dependent on the specific BTA–Cu^{+} bonding,[9] which restricted the adaptability of such a controlled release system to other applications. Supramolecular nanovalves based on pseudorotaxanes can regulate the release of a wide range of functional cargoes.[10] However, their high cost of the building blocks (*e.g.* price of cucurbituril hydrate[7] is 1250 £ per g, Aldrich) and complicated procedures fail in realizing the scaling-up production. We can figure out the key factors that support a feedback controlled release system to be applicable in fields other than pharmacology or molecular biology: a simple procedure, low-cost raw materials, high adaptability and effectiveness in controlling the release.

In this communication, we report a facile and cost-effective strategy for forming a pH-sensitive release system, which detains functional cargo within the nanocontainers at a neutral pH, and releases it in an acidic environment at a rate dependent on the pH value. Fig. 1a shows a nanovalve system consisting of two components: (1) a three-dimensional (3D) porous cobalt carbonate nanoprecipitate formed by spraying $Co(NO_3)_2$ (0.1 M) and Na_2CO_3 (0.2 M) solutions on the loaded nanocontainers, and (2) ethylenediamine triacetate chelating agent immobilized at the orifice of silica MCM-41 nanoparticles *via* a one-step reaction to stabilize the nanovalves. Fig. 1b shows high angle annular dark-field scanning transmission electron microscopy (HAADF-STEM) images and elemental mapping of loaded MCM-41 nanoparticles with nanovalves at their surfaces. The Co mapping confirms the distribution of the cobalt signal over the surface of the particles. In addition, the high contrast of the carbon distribution between the particle surface and the carbon grid underneath confirms the

[a] *Stephenson Institute for Renewable Energy, University of Liverpool, Liverpool, L69 7ZD, UK. E-mail: d.shchukin@liverpool.ac.uk, zzlwudi@liverpool.ac.uk*
[b] *Fritz-Haber-Institut, Faradayweg 4-6, 14195, Berlin, Germany*

† Electronic supplementary information (ESI) available. See DOI: 10.1039/c4cc05597g

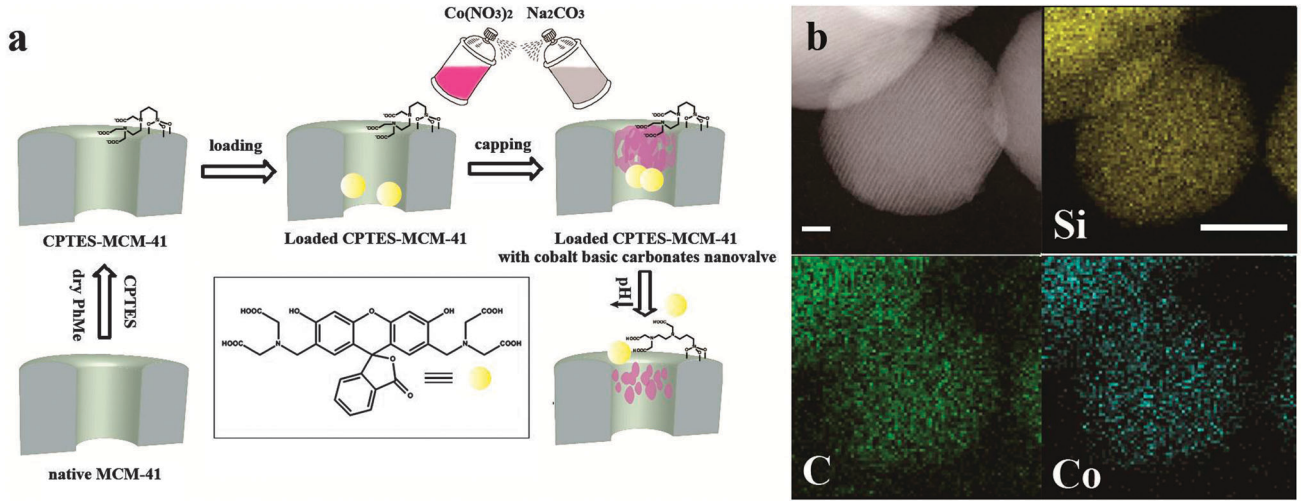

Fig. 1 (a) Schematic representation of the preparation and operation of acid responsive mechanized nanocontainers. (b) HAADF-STEM and elemental mapping images of loaded MCM-41 nanoparticle with nanovalves at the surface. Silicon, carbon and cobalt elemental maps are shown. Scale bar: HAADF-STEM 50 nm, elemental mapping 100 nm.

presence of chelating agents and nanovalves. We compared the nanocontainers functionalized with ethylenediamine-triacetate, ethylenediamine-4-oxo-2-butenoic acid salt and diethylenetriamine moieties in Table S1 (ESI†). The organic content is intentionally tailored to be approximately 0.2 mmol g^{-1}. Among the three samples, the ethylenediamine-triacetate-functionalized nanocontainers exhibited the highest Co content at 1.7 wt%, as estimated by energy-dispersive X-ray spectroscopy (EDX), which is consistent with the highest stability constant value of the Co–ethylenediaminetetraacetate complex ($\lg K_{stab}$ = 16.21) compared with the Co–acetic acid (2.24) and the Co–ethylenediamine (13.8).[11]

N_2 adsorption–desorption analysis confirms the one-step carboxylation of the silica nanocontainers, yielding a reasonably decreased BET surface area of 791.9 m^2 g^{-1}, pore diameter of 2.8 nm and pore volume of 0.63 m^3 g^{-1}, as compared with the native MCM-41 (Table S2, ESI†). The low carboxylate functionalization content of 0.23 mmol g^{-1} (as determined by TGA) not detected by FTIR, but confirmed by the negative ξ-potential (−45.3 mV). Furthermore, the consumption of *N*-(trimethoxy silylpropyl)-ethylenediamine triacetic acid trisodium salt solution (CPTES, 45 wt% in water) is only 0.07 mL per gram of native MCM-41, which is considerably lower than in other studies.[12] Small angle X-ray scattering (SAXS) reveals that the regular mesoporous structure of MCM-41 nanocontainers is roughly preserved after the carboxylation and formation of nanovalves (Fig. S1, ESI†).

The basic cobalt carbonate nanovalve with a 3D porous structure was formed by the quick complexation between divalent cobalt ions and the carbonate–hydroxide mixture.[13] The amorphous phase of the carboxylate-functionalized MCM-41 and unstable structure make it difficult to directly detect the structure under the high energy beam of microscopy techniques. Thus, we focused on the bulk gelatinous precipitates formed by a quick reaction between $Co(NO_3)_2$ (0.1 M) and Na_2CO_3 (0.2 M) solutions (Fig. 2a left). Higher and lower concentrations of spraying solutions have also been considered (ESI†). The resulting magenta product maintained a gel-like state after aging for three days, although nearly a 50% decrease in volume was detected (Fig. 2a right). The broad equivalence point recognition criteria (ERC) peak observed in the pH range of 6 to 2 in titration experiments indicates that the nanovalves contain a mixture of $CoCO_3$ and $Co(OH)_2$, which enables them to respond to a decrease in the pH by a gradual dissolution of the valve structure (Fig. 2b). Furthermore, the three-days-aged precipitates maintain a stable amorphous state without detectable crystallization, which can be confirmed by XRD (Fig. 2c). Fig. 2d (SAXS measurements) revealed two successive power-law regimes in the Porod region[14] of the gelatinous precipitates after 3 days aging, with a mass fractal regime (d_f = 2.3) and a surface fractal regime (d_s = 2.7) because the slopes are 2.3 and 3.3, respectively. SAXS pattern after 1 day aging (Fig. 2d) showed dual-size distributed aggregates with smaller slopes indicating an intermediate state of a 3D porous structure (ESI†). Longer aging times (*e.g.* 10 days) did not further increase the slopes of the precipitates (Fig. S2, ESI†) reflecting the structural stability of the nanovalves. The crossover occurs at K = 0.12 $Å^{-1}$, corresponding to a backbone thickness of K^{-1} = 8.3 Å. Schaefer and Keefer[15] concluded that such a structure is a 3D aggregate with rough pores and fractal backbones. The highly porous structure and the thinnest backbones of the basic cobalt carbonates ever reported can be attributed to the amorphous phase derived from the rapid complexation process.[16] The radius of gyration of the nanovalve is predicted to be approximately 22 Å by measuring the Guinier radius of the initial curvature of the SAXS curve[17] (Fig. S3, ESI†), which matches the pore diameter of the functionalized silica orifice. It is also noteworthy that a relatively large surface area (75.28 m^2 g^{-1}) of the bulk basic cobalt carbonates is preserved from coarsening by the 3D porous structure, which is in agreement with the observation in Fig. 2a. Therefore, it is reasonable to adopt basic cobalt carbonates as nanovalves because of their stable and porous structure and suitable size.

Calcein was selected for pH detection as a model cargo molecule in our work because of its chemical and optical properties. First, aggregated calcein emits weak fluorescence when confined within a mesopore, but when diffused in a bulk aqueous solutions can yield a strong fluorescence emission, which allows a reduction in the cargo loading. Second, the fluorescence emission of calcein is almost

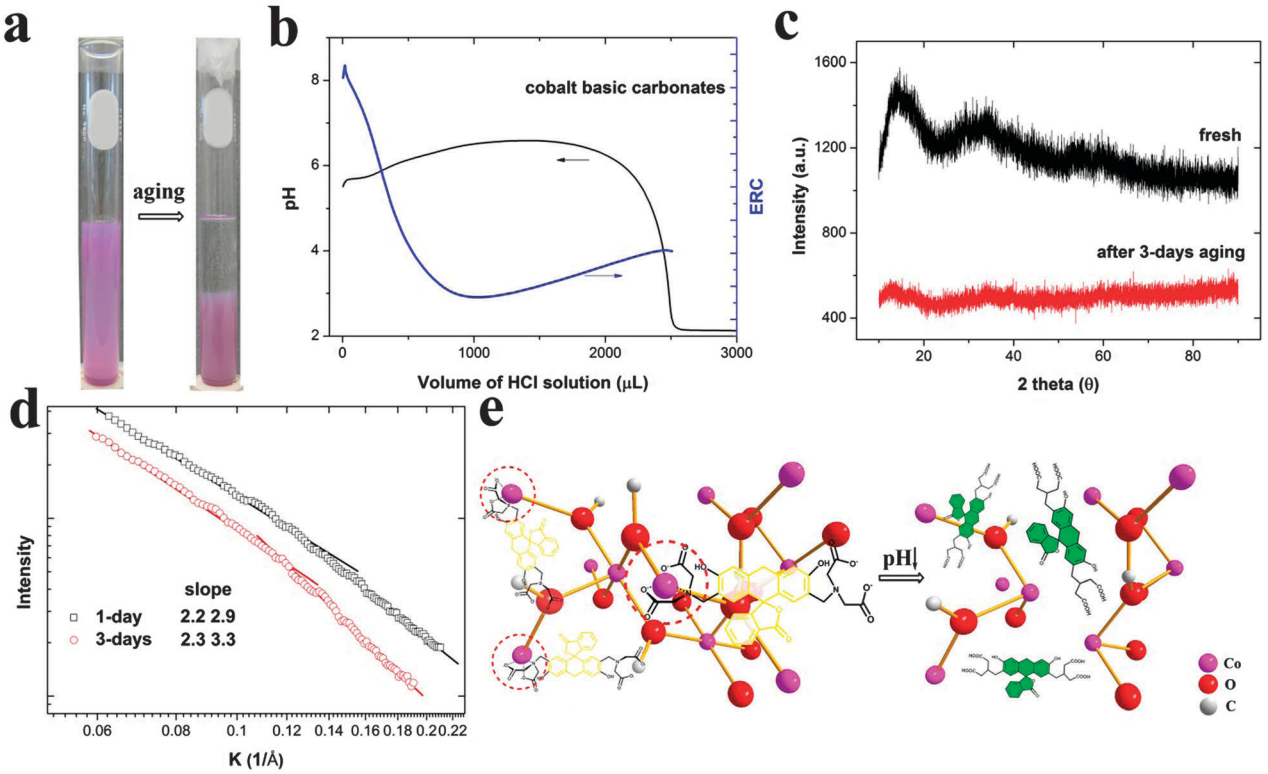

Fig. 2 (a) Comparison of cobalt basic carbonate precipitates between the beginning stage of flocculation and aging for three days under atmospheric pressure and at room temperature. (b) Titration and exothermic profile of cobalt basic carbonate precipitates. (c) XRD spectra of fresh basic cobalt carbonate precipitates and those after three-day aging. (d) Porod plots and the corresponding slopes of samples undergoing 1 and 3 days of aging at room temperature. (e) The two representations are modified from the crystal structure of $CoCO_3$ to highlight the chelating complexation between the calcein and the nanovalve, as well as the acid-induced partial and gradual dissolution of the valve structure and the dissociation of Co^{2+}–calcein complex bonds. The representations also reveal that the detained calcein cargo emits a weak fluorescence, but yield strong green emission when it is released from the nanovalve.

independent of the pH.[18] Third, Fig. 2e highlights that Co^{2+} can form a stable complex with a single iminodiacetic acid end group with a stability constant ($\lg K_{stab}$) of approximately 7.[19] For a pair of end groups, the value is 16.21, which helps to detain the cargo *via* the basic cobalt carbonate nanovalve. The 3D porous nanovalve provides a large number of unsheltered Co^{2+} centers because of the amorphous state and the relatively large surface area, which also facilitates the strong chelating complexation. Such complex bonds usually deform in response to a decrease in the pH because of the protonation of the electron donating agents. Thus, the controlled release system that is sensitive to the acidity of the bulk solution can be constructed with inherent pH-sensitivity of the basic cobalt carbonate nanovalve and complex bonds (Fig. 2e, right panel). The 3D porous nanovalves that detain the calcein molecules *via* chelating complexation can be partially and gradually dissolved as the pH value decreases. At the same time, the pH sensitive chelating complexation can also be dissociated because of the protonation of the complexing agents. Calcein molecules can yield a strong fluorescence emission in a bulk aqueous solution when the nanovalves are opened and the cargo is released.

Fig. 3a shows the pH-sensitive release of calcein cargo. Compared with the release profile without nanovalves in a neutral environment, the flat baseline confirms the effective detaining effect offered by the nanovalve; thus, the negligible premature leakage of calcein. The results indicate that the nanovalve can keep calcein over a long serving time under neutral conditions and release it as a feedback to an external trigger when necessary. The lag phase at the initial stage of release at pH = 5 indicates a slow process of dissolving nanovalves in such a weakly acidic environment. A burst release of the dye without any waiting time can be obtained when the surrounding medium is further acidified to pH = 4. The notable difference in response to the pH value may help us to detect the pH of polluted water sources in a rapid and direct way. We examined the influence of the ionic strength, concentration of transition metal ions and chelating anions (ethylenediaminetetraacetic acid (EDTA)) on the pH sensitivity. As shown in Fig. S4 (ESI†), the premature leakage of loading calcein in a neutral solution becomes obvious when the concentration of $NaNO_3$ is increased to 0.2 mol L^{-1}. The release of the cargo molecules is further accelerated under acidic conditions at a high ionic strength. Fluorescence spectroscopy can detect the pH-sensitive release at pH = 5 when the concentration of the transition metal ions (Cu^{2+}, Zn^{2+}, Fe^{2+} and Mn^{2+}) is below 0.5 mg L^{-1} (Fig. S4, ESI†). Our pH-responsive system can resist an EDTA concentration of up to 1500 ppb, which is higher than the safe upper-limit of the UK rivers (1120 ppb).[20] The nanovalve can also control the release of other cargo that forms a strong complex with divalent cobalt ions. For example, benzotriazole forms a stable complex with Co^{2+} and can also be released from the nanocontainers in response to a pH change (Fig. S5, ESI†). The resulting controlled release system has potential application in self-healing anticorrosion coatings.

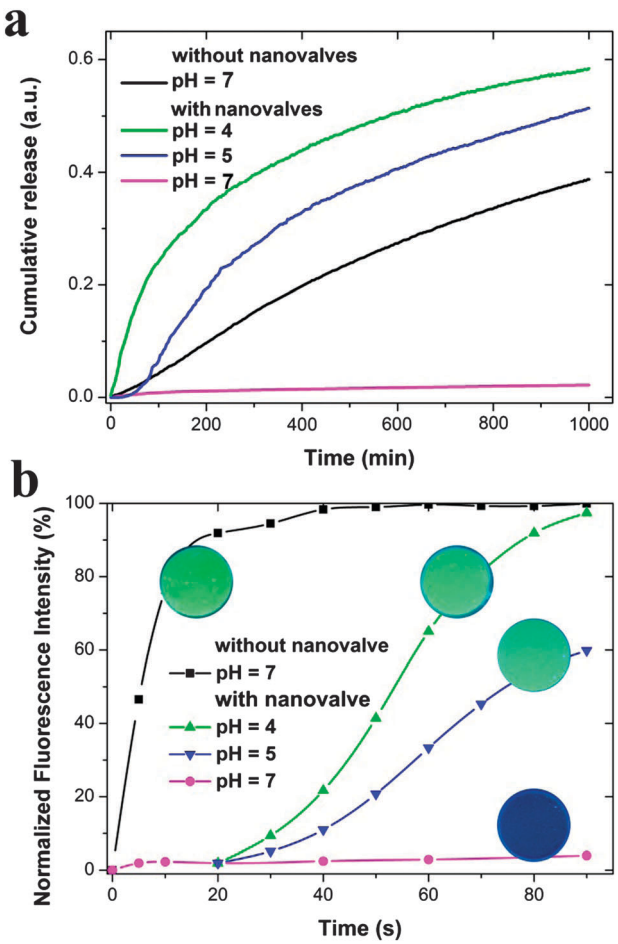

Fig. 3 (a) Release profile of calcein from loaded nanocontainers with Co–carbonate nanovalves. (b) Fluorescence intensity of the tablets as a function of time. The intensity was analysed using Leica's fluorescence software and normalized to the equilibrium intensity of the sample with uncapped calcein-loaded nanocontainers. The inset image (1) implies that the loaded containers with Co–carbonate nanovalves exhibit no emission at a neutral pH. The green fluorescence can be observed within 60 s at pH = 5 (2) and 10 s at pH = 4 (3). The inset image (1) represents the tablet containing calcein loaded containers without Co–carbonate nanovalves, which exhibits green fluorescence immediately after immersion in water at a neutral pH. The diameter of the tablets is approximately 10 mm.

For achieving our goal of scaling up the fabrication of containers with basic cobalt carbonate nanovalves for environmental detection, we pressed into tablets a mixture of aluminum oxide and calcein-loaded containers both in the presence and absence of Co–carbonate nanovalves (Fig. S6, ESI†) for pH detection. Inset image (1) in Fig. 3b reveals that the tablet containing the capped nanocontainers is colorless under neutral conditions, but exhibits a green emission in an acidic environment. The color can be visibly detected within 1 min at pH = 5 and within only 10 s at pH = 4 (inset images (2) and (3), respectively). The notable difference in pH responsive green fluorescence can help to quickly estimate the pH value of the water source. In contrast, the uncapped nanocontainers immediately release calcein after their immersion in water at a neutral pH (inset image (4)). In addition, the fluorescence intensity at the edge part of the tablets was also recorded. Fig. 3b reveals that a tablet with capped nanocontainers emits a very weak fluorescence after immersion under neutral conditions for 20 s. Once it has been moved to an environment with pH = 5, the intensity gradually increases with time. During the same period, the nanovalve structure would be further dissolved in pH = 4, which results in a quicker release of calcein and the fluorescence intensity reaches a saturated level within only 90 s. Using this easy to handle product, we can also detect our working and living environmental condition. The tablets exhibit invisible green emission after a 20 s immersion in water samples collected from university campus and the residential area near a food factory (Fig. S7, ESI†), implying a safe outdoor environmental quality for people to enjoy their working and living spaces. The pH values of the wild water samples were then confirmed to be 7.4 using a pH meter in the university campus and 7.0 near the food factory.

In summary, we demonstrated a facile and cost-effective method to fabricate a pH-sensitive release nanovalve system that has the advantages of simple synthesis, low-cost raw materials, high adaptability and effectiveness in controlling the release. The basic cobalt carbonate nanovalves exhibit effective control over cargo storage and release at different pH ranges. The proposed nanovalves can be easily up-scaled to substantial quantities for their implementation in fields requiring storage and controlled release under the conditions different from the *in vivo* environment.

We thank Ingrid Zenke at the MPI-KGF (Golm, Germany) for the SAXS measurements. This work was financially supported by the Brian Mercer Feasibility Award from Royal Society of Chemistry, UK.

Notes and references

1 C. Alvarez-Lorenzo and A. Concheiro, *Chem. Commun.*, 2014, **50**, 7743.
2 A. Bortolin, F. A. Aouada, M. R. de Moura, C. Ribeiro, E. Longo and L. H. C. Mattoso, *J. Appl. Polym. Sci.*, 2012, **123**, 2291; X. J. Wang and J. Zhao, *J. Agric. Food Chem.*, 2013, **61**, 3789.
3 J. J. Fu, T. Chen, M. D. Wang, N. W. Yang, S. N. Li, Y. Wang and X. D. Liu, *ACS Nano*, 2013, **7**, 11397; Y. Le, P. T. Hou, J. X. Wang and J. F. Chen, *Mater. Chem. Phys.*, 2010, **120**, 351.
4 D. M. Liu, K. D. Lu, C. Poon and W. B. Lin, *Inorg. Chem.*, 2014, **53**, 1916.
5 H.-W. Gao and X.-H. Xu, *Chem. Commun.*, 2011, **48**, 12810.
6 E. Abdullayev, V. Abbasov, A. Tursunbayeva, V. Portnov, H. Ibrahimov, G. Mukhtarova and Y. Lvov, *ACS Appl. Mater. Interfaces*, 2013, **5**, 4464.
7 D. Tarn, M. Xue and J. I. Zink, *Inorg. Chem.*, 2013, **52**, 2044.
8 E. Abdullayev and Y. Lvov, *J. Mater. Chem.*, 2010, **20**, 6681.
9 Y. Li, M. L. Gong, K. Ramji and Y. Z. Li, *J. Phys. Chem. C*, 2009, **113**, 18003.
10 M. Li, H. Yan, C. Teh, V. Korzh and Y. Zhao, *Chem. Commun.*, 2014, **50**, 9745; M. W. Ambrogio, C. R. Thomas, Y.-L. Zhao, J. I. Zink and J. F. Stoddart, *Acc. Chem. Res.*, 2011, **44**, 903.
11 T. E. Furia, *CRC Handbook of Food Additives*, Taylor & Francis, 2nd edn, 1980, ch. 6.
12 D. He, X. He, K. Wang, Y. Zhao and Z. Zou, *Langmuir*, 2013, **29**, 5896.
13 R. Xu and H. C. Zeng, *J. Phys. Chem. B*, 2003, **107**, 12643.
14 D. W. Schaefer, A. J. Hurd, D. K. Christen, S. Spooner and J. S. Lin, *MRS Online Proc. Libr.*, 1988, **121**, DOI: 10.1557/PROC-121-305.
15 D. W. Schaefer and K. D. Keefer, *Phys. Rev. Lett.*, 1986, **56**, 2199.
16 W. D. Kingery, H. K. Bowen and D. R. Uhlmann, *Introduction to ceramics*, Wiley, 1976.
17 C. J. Brinker, K. D. Keefer, D. W. Schaefer and C. S. Ashley, *J. Non-Cryst. Solids*, 1982, **48**, 47.
18 J. S. Liu and X. Z. Du, *J. Mater. Chem.*, 2010, **20**, 3642.
19 G. Schwarzenbach, G. Anderegg, W. Schneider and H. Senn, *Helv. Chim. Acta*, 1955, **38**, 1147.
20 EDTA environment safety standards. Available online: http://www.epa.gov/opprd001/inerts/edta.pdf.